Evaluate the impact of a 4-hour tandem phase on the continuity of nadir altimetry measurements between S3 and S3NG-T

Noémie Lalau[1], Michaël Ablain[1], Thomas Vaujour[1], François Boy[2], Gerald Dibarboure[2], and Alejandro Egido[3]

[1]MAGELLIUM, Ramonville Saint-Agne, 31520, France
[2]CNES, Toulouse, 31400, France
[3]ESA, ESTEC, Noordwijk, 2201 AZ, The Netherlands

Correspondence: Noémie Lalau (noemie.lalau@magellium.fr)

Abstract. The upcoming Sentinel-3 Next Generation Topography (S3NG-T) mission, designed to succeed the current Sentinel-3 (S3) mission, will operate on the same ground tracks as the current S3 constellation to maximise continuity of measurements, but with a fixed 4-hour temporal lag due to satellite design constraints. This configuration prevents the implementation of a classical near-simultaneous tandem phase, traditionally used for inter-mission cross-calibration, and raises concerns regarding the impact of short-term oceanic variability on continuity assessment.

In this study, we evaluate the feasibility and expected performance of a 4-hour delayed tandem phase for cross-calibrating S3 and S3NG-T. Using tandem datasets from Sentinel-3A/B and Jason-3/Sentinel-6 missions, combined with SWOT KaRIn observations, we develop a methodology to quantify the oceanic variability introduced by a 4-hour delay and to evaluate its effect on the accuracy of inter-mission offset estimates.

Results indicate that the classical tandem configuration achieves regional inter-mission Sea Level Anomaly (SLA) offset uncertainties of approximately 2 mm over a three-month period. In contrast, a 4-hour delayed tandem phase increases this uncertainty to about 7 mm in the same period, but still performs significantly better than non-tandem scenarios. Extending the 4-hour tandem phase to one year enables the detection of systematic instrumental errors of ±3.5 mm amplitude, sufficient to ensure continuity between S3 and S3NG-T. These findings demonstrate that, despite additional oceanic variability, a 4-hour tandem configuration remains a viable and effective strategy for cross-calibration, especially when supported by improved environmental corrections and ~~extended observation duration~~ by extending the observation duration to a full year.

1 Introduction

The Sentinel-3 (S3) and Sentinel-3 Next Generation Topography (S3NG-T) missions are part of the Copernicus Programme led by the European Commission. The European Space Agency (ESA), is mandated to define the Copernicus space component (CSC) architecture based on user requirements coordinated by the Commission, in collaboration with EUMETSAT, and Member States. The S3 and S3NG-T missions aim at providing continuous, high-accuracy measurements of sea surface topography, sea and land surface temperature, and ocean and land surface colour. S3 plays a central role in supporting operational oceanography, environmental monitoring, and long-term climate records. Looking ahead to the 2030–2050 timeframe, the S3NG-T mission primary objective is to ensure the continuity of the existing Copernicus S3 nadir-altimeter measurements with enhanced performance, coverage and revisit time (European Space Agency, 2025).

The S3NG-T mission consists of two large ~~spacecrafts~~ spacecraft equipped with an across-track interferometer swath altimeter (SAOOH), a synthetic aperture radar (SAR) nadir altimeter (Poseidon-5), a multi-channel microwave radiometer, and a precise orbit determination suite. The two spacecrafts will fly in a sun-synchronous orbit at ~~6pm~~ 6 pm local time ascending node (LTAN), at a mean orbital height of 815 km, with an orbital phase difference of 140°, achieving an interleaved groundtrack between both satellites, and matching the Sentinel3A/3B ground tracks. Since S3NG-T satellites will be of a new design, it is imperative that the characteristics of the new system are introduced into the S3 time series in a manner that does not introduce instability into the long time series.

To achieve the primary objective of ensuring the continuity of S3 topographic measurements, it is essential to have a successful cross-calibration between the current S3 constellation and the S3NG-T mission. The most effective method for accurately assessing continuity between successive altimeter missions over the ocean is the tandem flight phase (hereafter referred to as 'tandem phase'). During a tandem phase, two successive missions follow an identical ground track separated by a strictly controlled time interval. Tandem phases have been systematically implemented following the launch of new reference altimetry missions, including TOPEX-Poseidon and Jason-1 (2002; 70-second gap), Jason-1 and Jason-2 (2008; 55-second gap), Jason-2 and Jason-3 (2016; 80-second gap), and Jason-3 and Sentinel-6 Michael Freilich (2021-2022; 30-second gap). They have also been used between non-reference missions, such as ERS-2 / Envisat (2007-2008, 2010-2011; 30-minute gap) and Sentinel-3A and Sentinel-3B (2018; 30-second gap). This S3A/B tandem phase allowed a precise cross-calibration of the S3 constellation instruments (Rieu et al., 2021), supporting the generation of consistent and unbiased time-series observations for climate monitoring (Clerc et al., 2020), following the approach previously applied to the Jason series (Dibarboure et al., 2011). ~~During a tandem phase, two successive missions follow an identical ground track at intervals of less than one minute.~~ These calibration campaigns are essential for maintaining the accuracy and stability of the satellite altimetry record (Dorandeu et al., 2004; Leuliette et al., 2004; Zawadzki and Ablain, 2016). The significant benefits of a tandem phase have been thoroughly explained by Ablain et al. (2025). A key assumption during this period is that the ocean and atmospheric conditions, at the scales of interest, do not vary significantly between measurements made by the two altimetry missions. This allows for the cancellation of geophysical and atmospheric effects when comparing sea level measurements from the two altimeters. Consequently, the relative errors between altimetry missions, arising from instrumental differences (e.g., altimeter noise), data processing disparities (e.g., retracking algorithms), precise orbit determination, and variations in the mean sea surface, can be accurately determined. Averaging these differences over the entire tandem phase period enables ~~cancelation~~ cancellation of random effects, thereby allowing for the accurate determination of systematic instrumental errors between the two successive altimetry missions (Masters et al., 2012; Henry et al., 2014; Guérou et al., 2023).

The precise determination of these systematic sea level differences due to instrumental errors facilitates investigation of their origin and potential future correction. Furthermore, averaging these systematic sea level differences provides the mean sea level offset between two successive missions. This offset is essential for accurately linking the two successive altimeter missions, thereby ensuring a continuous sea level data record.

On the global scale, the mean sea level offset between two successive reference missions is calculated with an accuracy lower than 0.5 mm at a confidence level of 68% (Zawadzki and Ablain, 2016; Guérou et al., 2023). At regional scales of a few hundred km, the uncertainty of the mean sea level offset increases to 2 mm (update from Prandi et al. (2021)) depending on the area. These uncertainty levels, obtained during the tandem phase, demonstrate our ability to assess the sea level continuity on both global and regional scales between two successive altimetry missions, and represent the limit of detectability of systematic errors.

However, the standard tandem phase with a near-zero temporal lag will not be feasible between S3 and S3NG-T due to orbital constraint, with a 6:00 p.m. LTAN for S3NG-T and 10:00 p.m. LTAN for S3A/B. This configuration imposes a 4-hour time lag between the S3 and S3NG-T observations at the same location. As a result, the two altimeters will no longer observe the same oceanic surface simultaneously during their tandem phase. Even when spatially collocated, sea level measurements taken just four hours apart will differ significantly due to natural, high-frequency ocean processes. These include internal tides, internal waves, inertial motions, mesoscale eddies, and submesoscale dynamics, all of which induce significant fluctuations on sub-daily timescales (Dufau et al., 2016; Cronin et al., 2012). As a consequence, the introduction of ocean variability effects in the sea level differences calculated during a 4-hour tandem phase will reduce our ability to assess the sea level continuity between S3 and ~~S3NG~~S3NG-T.

This study aims to evaluate the impact of a 4-hour tandem phase on the continuity of sea level measurements provided between S3 and S3NG-T nadir altimetry measurements. To achieve this objective, we explore methods for quantifying the oceanic variability introduced by this 4-hour delay and evaluate potential strategies to ensure reliable continuity in the absence of a conventional tandem phase. The datasets used in this study are detailed in Section 2. Section 3.1 presents the method used to verify continuity and section 3.2 presents the methodology developed to quantify the ~~uncertainty associated~~ associated uncertainty. Section 3.3 describes the approach adopted to characterise the oceanic variability induced by the 4-hour lag. The main results are presented in Section 4, and additional comparisons with other methods and missions are discussed in Section 5.

2 Data

This study relies on altimetric missions with overlapping temporal coverage to evaluate tandem phases and quantify their impact on inter-mission continuity. The primary missions considered include Jason-3 (J3), Sentinel-6 Michael Freilich (S6A), Sentinel-3A (S3A), Sentinel-3B (S3B), and SWOT. These missions provide complementary datasets ~~across~~ for different orbits and tandem configurations.

The tandem phase between S3A and S3B serves as a proxy for the future configuration of Sentinel-3D and ~~S3NG~~S3NG-T. This phase represents a relevant case study of two satellites flying on the Sentinel-3 orbit and constitutes the core dataset from which the main results of this study are derived. The S3A/S3B tandem phase lasted from 7 June to 16 October 2018, spanning four complete 27-day cycles or ten 12-day sub-cycles, with a 30-second time interval between the satellites (Clerc et al., 2020).

For comparison, data from the J3 and S6A missions were used to analyse a longer tandem phase on a different orbit, enabling an application of the methodology beyond the Sentinel-3 constellation. The J3/S6A tandem phase extended from 17 December

2020 to 7 April 2022 and includes more than 40 cycles of 10 days, with also a 30-second time interval between the satellites. However, due to an anomaly on the Poseidon-4 altimeter (side A) shortly after the S6A launch, only the data acquired after the switch to side B ~~performed~~ , performed on 14 September ~~2021~~ 2021, were retained for this study (Dinardo et al., 2022).

In addition, SWOT KaRIn data were used to estimate the impact of natural oceanic variability on ~~SLA~~ Sea Level Anomaly (SLA) differences over a 4-hour time lag. SWOT was selected due to its dense network of ~~crossover~~ dual-crossover points with the S3A and S3B ground tracks, offering high spatial and temporal resolution, which is essential for characterising oceanic variability effects.

The data used in this study are publicly available. We ~~employed~~ used L2P 2024 products for J3, S6A, S3A ~~,~~ and S3B, and the SWOT KaRIn Science Phase data (Version 1.0.2). The SWOT Level-3 Low Rate SSH product ~~derived~~ , derived from the KaRIn L2 low-rate ocean ~~data~~ data, is produced by the AVISO and DUACS teams as part of the DESMOS Science Team project and is freely accessible via AVISO (AVISO/DUACS, 2024).

The L2P ~~contain~~ contains the along-track ~~sea level anomaly~~ SLA at 1Hz (~~SLA,~~ see Eq. 1) calculated after applying a validation process fully described in the product handbook of each altimetry mission ~~(Along-track Level-2+ (L2P) Sea Level Anomaly Sentinel-3 / Jason-CS-Sentinel-6 Product Handbook, 2022)~~(Sentinel-3 and Jason-CS-Sentinel-6 Product Handbook, 2022). The along-track SLA is derived from the following equation:

$$SLA = Orbit - Range - \Sigma_i Correction_i - MeanSeaSurface \qquad (1)$$

where $Orbit$ is the radial distance between the ~~satellites and the geoid~~satellite's center of mass and the reference ellipsoid, $Range$ the distance between the satellite and the sea surface, $\Sigma_i Correction_i$ are the sum of the geophysical and atmospheric corrections to be applied (e.g. ocean, polar and earth tides, wet and dry troposphere corrections, sea state bias correction,...), $MeanSeaSurface$ is the ~~mean of the~~ time-averaged sea surface height referenced to the ellipsoid, from which sea level anomalies are derived. The geophysical corrections applied in L2P products for the SLA calculation are already homogenised for each altimetry mission and identical during a tandem phase.

3 ~~Methods~~Method

3.1 Comparison between two missions

To evaluate the continuity of sea level measurements between two altimetric missions, we investigate in this study three distinct scenarios. The first is the classical tandem phase, in which the satellites follow each other closely in both space and time, allowing for nearly simultaneous co-located observations. The second scenario considers a configuration without any tandem phase, where sea level data from the two missions are ~~neither~~ co-located in neither time nor space. The third scenario simulates a delayed tandem phase ~~with a 4-hour temporal offset,~~ where measurements are co-located in space but ~~not in time (~~separated by a 4-hour time lag~~)~~. Each of these configurations presents different conditions for estimating the offset between missions, and consequently different associated uncertainties. By comparing the uncertainty in sea level differences across these three scenarios, we aim to assess the feasibility and accuracy of the 4-hour tandem phase as a substitute for the classical approach.

~~The method used to verify continuity is applicable to both tandem and non-tandem~~ We apply a unified processing method to assess measurement continuity across all three scenarios. For each ~~cycle of each~~ mission, along-track SLA data are aggregated ~~onto a regular spatial grid to produce gridded fields of mean sea level (MSL). These gridded fields, referred to as regional MSL grids, are constructed for each cycle (or subcycle in the case of S3) independently.~~

~~To homogenize comparisons~~ into regular 3° × 3° spatial grids to generate SLA grids. This specific 3° resolution was uniformly selected to minimise empty grid cells and optimise spatial coverage. To ensure a consistent comparison between missions with ~~different orbital characteristics , a consistent temporal window of 12 days -corresponding to three 4-day sub-cycles of the S3A/S3B orbit- was adopted for all configurations. This allows direct comparison between the~~ differing orbital characteristics (e.g., the 10-day ~~cycles~~ cycle of J3/S6A ~~and~~ versus the 27-day ~~cycles~~ cycle of S3A/S3B~~.~~

~~To ensure consistency in spatial resolution and optimise coverage, SLA data are binned into grid cells of 3°×3°. This resolution minimises the number of empty cells, particularly when considering~~), we adopted a fixed 12-day ~~subcycles for S3A and S3B. This 3° grid spacing is uniformly adopted in all scenarios and missions in this study.~~ temporal window for all configurations, corresponding to three 4-day sub-cycles of the S3 orbit. These gridded fields are computed independently for each 12-day period.

~~For each cycle,~~ From these SLA grids, we calculate the difference between the ~~regional MSL grids from the two missions is computed, resulting in~~ two missions for each 12-day window, yielding a series of ~~SLA difference maps~~ ΔSLA grids. By taking a weighted spatial average of each ~~difference map~~ ΔSLA grid, we obtain a time series of global mean ~~sea level (GMSL)~~ SLA differences between the two missions~~, with one value per cycle. The~~ . The temporal mean of this time series provides an estimate of the global mean SLA offset.

In addition to ~~this~~ the global assessment, ~~regional offsets are also evaluated. In~~ we evaluate regional SLA offsets to capture geographic variability. Within each grid cell, we extract a time series of ~~SLA differences is derived~~ the ΔSLA values across the observation period. The temporal ~~average of this time series yields a map of the regional~~ mean of these localised time series generates a spatially resolved map of regional SLA offsets. This ~~spatially resolved approach allows for the assessment of geographic variability in the offset and is particularly useful for analysing the effect of spatially~~ perspective is critical for analysing geographically dependent phenomena, such as regional instrument biases (Nilsson et al., 2022).

In this study, the focus is placed primarily on regional ~~offset estimation and its~~ SLA offset uncertainty. On a global scale, the impact of a 4-hour time lag is negligible due to the averaging of uncorrelated oceanic signals. However, at regional scales, such variability can introduce significant errors, making regional analyses crucial to understand the implications of the 4-hour tandem configuration.

To clarify the dataset, Table A1 summarises the individual SLA grids and the resulting ΔSLA grids generated across all missions and scenarios.

3.2 Uncertainty computation

Quantifying the uncertainty associated with regional ~~MSL (RMSL)~~ SLA offset estimates is essential for assessing the reliability of continuity verification methods. This uncertainty reflects the variability of differences observed across several repeat cycles and is evaluated separately for each of the three continuity scenarios described above. In this study, we consider two complementary approaches to quantify the uncertainty of regional offset estimates. The first method ~~provides~~ uses the spatial variance in regional SLA offsets to provide a single global uncertainty value~~based on the spatial variability~~ , capturing the overall spread of the regional ~~offset map, offering an integrated view of the spatial dispersion in offset~~ SLA offset estimates. The second method estimates ~~uncertainty locally~~ regional uncertainty at each grid point by analysing the temporal variability of SLA differences ~~, while also accounting for potential autocorrelation in~~ between two missions. This approach incorporates the autocorrelation structure of the time series to ensure more realistic uncertainty estimates. These two methods offer distinct yet complementary perspectives -spatial versus temporal- and together provide a more robust and comprehensive assessment of uncertainty under varying observational configurations.

3.2.1 Spatial ~~standard deviation of RMSL offset maps~~method

The method described in Section 3.1 for comparing missions produces ~~a map of RMSL differences~~ ΔSLA grids for each cycle. The temporal mean of these cycle-by-cycle differences is then computed for each grid cell. This temporal average, ~~$\Delta MSL(lat,lon)_{n\_cycle}$~~$\overline{\Delta SLA}(lat,lon)_{n\_cycle}$, represents the ~~RMSL~~ regional SLA offset between the two missions over "n" cycles. This average can be computed during or outside the tandem phase. The uncertainty associated with the ~~RMSL~~ regional SLA offset is then quantified as the standard deviation of the spatial variations of this temporal mean. This standard deviation, denoted as

$$u = \sigma(\Delta MSL \overline{\Delta SLA}(lat,lon)_{n\_cycle})$$

provides an estimate of the ~~RMSL~~ regional SLA offset uncertainty relative to the global mean. The uncertainty derived from this methodology assumes that the ~~RMSL differences~~ $\overline{\Delta SLA}(lat,lon)$ grid represent N independent ~~realizations~~ realisations of the offset error. By verifying that the distribution of these differences follows a Gaussian distribution, the standard deviation can be interpreted as a 1-σ uncertainty. To ensure this estimate is realistic, it is crucial to correct for any detectable systematic effects before performing the calculations. Uncorrected systematic errors could inflate the standard deviation, leading to an overestimation of the uncertainty.

3.2.2 ~~Regional offset uncertainty~~Temporal method

Another way to calculate the uncertainty of the ~~RMSL~~ regional SLA offset is to compute the standard deviation of each temporal time series of ~~MSL at regional scales~~SLA in each grid cell, as proposed by Prandi et al. (2021):

$$\sigma(lat,lon)_{n\_cycle} = \sigma(\Delta MSL \Delta SLA_{lat,lon}(t))$$

The uncertainty for each grid cell is then computed using the formula from Guérou et al. (2023):

$$u = t^{n-1}_{1-\alpha/2} \frac{\sigma_{lon,lat}}{\sqrt{n'}} \quad (2)$$

and

$$n' = \frac{1-\rho_1}{1+\rho_1} n_{sample} \quad (3)$$

Where σ is the standard deviation of the sample ; n is the number of measurements ; t is the Student's coefficient for (n - 1) degrees of freedom and a confidence level of α ; n' is the effective sample size, accounting for any autocorrelation in the data.

Unlike the previous approach, which estimates a single regional offset uncertainty relative to the global mean, this method calculates the uncertainty of each local offset. However, for this study, the small sample size during the tandem phase limits the accuracy of n'.

3.3 Accounting for 4-hour variability

To quantify the variance of oceanic variability and measurement errors over short time intervals, we analysed ~~crossover~~ dual-crossover differences between SWOT's KaRIn swath data and Sentinel-3A/3B nadir data (~~ΔSSHA~~ΔSLA). This analysis is based on almost one year of data from SWOT's science phase, leveraging a high number of ~~crossovers~~ dual-crossovers and an extensive spatial coverage. A ~~crossover~~ dual-crossover is defined as the intersection of ground tracks from two different satellites, enabling the comparison of spatially colocated measurements, although acquired at different times.

3.3.1 ~~Estimation of 4-hour variability~~

The first step involves constructing a map of ~~ΔSSHA variance for crossovers~~ ΔSLA variance for dual-crossovers with time interval of $\Delta t = 4$ hours, using data aggregated into 5° × 5° grid cells. This map captures high-frequency oceanic variability, systematic errors, and altimeter noise, represented as: $\sigma^2 = {\sigma^2}_{ocean} + {\sigma_{SWOT}}^2 + {\sigma_{S3}}^2$ where ${\sigma^2}_{ocean}$ accounts for oceanic variability and ~~${\sigma_{SWOT}}^2, {\sigma_{S3}}^2$~~ ${\sigma_{SWOT}}^2, {\sigma_{S3}}^2$ represent the systematic errors and instrumental noise for SWOT and Sentinel-3, respectively.

The second step consists of generating a variance map for Δt approaching 0 hours, where the contribution of oceanic variability is negligible. This map isolates systematic errors and altimeter noise in the ~~$\Delta SSHA$~~ ΔSLA measurements, providing a baseline against which to compare the 4-hour map. Both maps are processed using a mean filter followed by interpolation to fill data gaps and oversampling to a finer 3° × 3° resolution. By subtracting the 0-hour variance map from the 4-hour variance map, an upper bound on the variance associated with 4-hour oceanic variability is obtained. This estimate constitutes an upper bound because the calculation may still include residual instrumental and environmental correction errors. The variance associated with altimeter noise is assumed to be time-invariant and therefore cancels out in the subtraction. The resulting variance map is expressed in terms of ${\sigma_{i,j}}^2$, representing the variance within each 3° × 3° grid cell. ~~This map~~

This spatial distribution, represented in the left panel of Fig. 1, reveals spatial heterogeneities in the variance of ~~$\Delta SSHA$~~ΔSLA. Notable high values are observed in regions such as the Madagascar Basin, the British Isles and the Indonesian archipelago~~(see Fig. ??) .~~. These regions are characterised by large tidal amplitudes or complex coastal dynamics. To better understand the origin of this variance, the right panel of Fig. 1 illustrates the evolution of the cumulated variance (σ^2) of the ΔSLA at dual-crossover points as a function of the time delay Δt. The systematic errors and instrumental noise for SWOT and Sentinel-3 represented in grey are assumed to be constant over time. The contribution of oceanic variability represented in blue increases rapidly. Specifically, the temporal evolution is not purely linear or random. It exhibits distinct modulations, with a visible signature around 12 hours and more pronounced oscillations with a period of approximately 24 hours. The correlation between these temporal signatures (diurnal and semi-diurnal) and the coastal areas of high variance observed in the left panel of Fig. 1 indicates that this high-frequency variance is not driven solely by true physical ocean dynamics. It also clearly illustrates the presence of residual errors in the environmental corrections, particularly in tide models.

3.3.1 ~~Propagation of variability into offset uncertainty~~

To simulate the impact of additional sea-level variance due to a 4-hour tandem phase, random error grids are introduced into the observed ~~SSHA~~ SLA differences during the tandem phase. The $3° \times 3°$ grid variance map is used to generate regional random error grids. For each cycle, a random error grid is constructed following a normal distribution with variance ~~$\sigma_{i,j}$~~$\sigma_{i,j}{}^2$. These regional error grids are then added to the ~~observed SSHA differences during the tandem phase of Sentinel-3A and Sentinel-3B~~ΔSLA grids of S3A and S3B tandem phase. The offset uncertainty is then computed on this new dataset applying the same methodology as described in Section 3.2.

This approach was preferred to the use of a global Ocean General Circulation Model (OGCM) or operational model hindcasts, as they struggle to faithfully represent true high-frequency ocean variability. The variability introduced over a short 4-hour delay is heavily dominated by high-frequency, sub-daily ocean dynamics, specifically internal gravity waves, internal tides, and sub-mesoscale eddies. While state-of-the-art global ocean models successfully reproduce large-scale mesoscale circulation, accurately resolving the exact global phase and amplitude of these specific high-frequency signals remains a significant modelling challenge. New ultra-high-resolution experimental models, built on the MITgcm framework, are now capable of capturing internal tides and high-frequency sub-mesoscale structures. However, these currently remain advanced research tools rather than standard operational global hindcasts. Therefore, relying on actual recorded satellite altimeter datasets was considered the most appropriate and robust approach to capture the true physical noise floor. Specifically, the SWOT mission resolves kilometer-scale SLA structures across a 120-km swath (Morrow et al., 2019; Archer et al., 2025), enabling a fair representation of the sub-mesoscale structure. For instance, while small-scale waves such as long-crested solitons can be reproduced in ultra-high-resolution models like a 1/50° HYCOM simulation, these simulations still under resolve the true abundance and complexity of small-scale features that are directly captured by SWOT (Buijsman et al., 2026).

4 Results~~: Classic tandem vs. 4-hour tandem phase~~

In this section, we compare the continuity performance of three configurations: the classical S3A/S3B tandem phase with a 30-second time interval, a 4-hour delayed tandem configuration, and a non-tandem scenario exploiting S3A and S3B data acquired after their tandem phase. The analysis is conducted using along-track comparison methods over a $3° \times 3°$ grid with 12-day sub-cycles, as described in Section 3.1. The uncertainty presented in these results is computed using the temporal method, which is based on analysing the temporal variability of the ΔSLA grids within each grid cell, as described in Section 3.2.2. As shown in Fig. ~~??~~2, over a period of ten 12-day ~~cycles~~ sub-cycles (approximately four months), the regional inter-mission ~~bias~~ offset uncertainty is estimated at 2 mm in the classical tandem phase, compared to 7 mm for the 4-hour delayed tandem and 10.5 mm in the non-tandem scenario -representing three and five times higher uncertainty, respectively.

These results underscore the advantage of close ~~spatiotemporal~~ spatio-temporal co-location in reducing the measurement noise and improving the inter-mission ~~bias~~ offset precision. As expected, the uncertainty in the ~~bias~~ offset estimate decreases with the number of tandem cycles, primarily due to the averaging of random errors. The ~~tandem phase also enables a more~~ classical tandem phase enables highly effective detection of systematic ~~errors, as the oceanic variability is minimized. These systematic errors are~~ differences mainly due to instrumental errors by minimising the effect of differences in oceanic variability. These spatially correlated systematic differences are clearly visible on the regional ~~offset map during the tandem phase (see Fig. ??), but they are noisier with~~ SLA offset map in panel (a) of Fig. 3. Notably, a distinctive positive offset (up to 7 mm) dominates the high southern latitudes (south of 30°S). This can likely be attributed to differences in how the two altimeters' retracking algorithms process Sea State Bias (SSB), as the Southern Ocean is characterised by high Significant Wave Heights (SWH). These zonal patterns are significantly harder to detect in panel (b), demonstrating how the oceanic variability differences introduced by a 4-hour delay masks underlying instrumental errors. In the non-tandem configuration, these same systematic patterns begin to emerge only after one year of observation, with amplitudes reaching up to 6 mm.

While the 4-hour temporal lag introduces additional variability, the resulting uncertainty remains significantly lower than in the absence of any tandem overlap. This demonstrates that even partial co-location~~such~~, such as with a few hours of ~~delay~~ delay, can significantly improve the reliability of continuity assessments.

5 Assessment

This section evaluates the robustness and general applicability of the proposed continuity assessment framework. Specifically, we investigate three complementary aspects: (1) the consistency of results when applied to a different pair of altimetric missions, namely J3 and S6A; (2) the sensitivity of the along-track comparison methodology, evaluated through comparison with a ~~crossover-based~~ dual-crossover-based approach; and (3) the consistency of regional uncertainty estimates obtained from two distinct statistical methods. Together, these analyses allow us to test the validity, flexibility, and limitations of the proposed methodology under varying mission configurations and observational constraints.

5.1 Comparison with J3/S6A missions

To validate the robustness of our findings, we performed a comparative analysis using J3 and S6A missions (see Fig. ~~??~~4), which are on a different orbit than S3A and S3B. The uncertainty presented in this comparison is computed using the temporal method described in Section 3.2.2. These two missions also benefited from a tandem phase, offering an opportunity to verify the performance observed with the S3A/S3B configuration. Results confirm that orbital characteristics do not significantly affect the ability to detect inter-mission offsets during tandem phases, thereby validating the method across different mission pairs.

Outside the tandem phase, however, the orbital configuration becomes a critical factor. After one year of data, the uncertainty ranges from 6 mm for S3A/S3B to 12 mm for J3/S6A. The reference mission orbit (used by TOPEX, the Jason series, and S6A) has a 9.9-day repeat cycle and a ground track separation of 314 km at the equator. In a two-satellite configuration~~such~~, such as J3 and S6A , where J3 is placed on an interleaved orbit following the tandem phase phase, the inter-track separation at the equator is reduced from 314 km to 157 km after one full cycle. For S3A/S3B's configuration, this separation is reduced from 104 km to 52 km, reducing the impact of oceanic variability. The offset uncertainty observed in these non-tandem conditions is highly sensitive to such geometric configurations.

5.2 Sensitivity Analysis of the Along-Track Method: Comparison with Crossover-Based Approach

Beyond validating the S3A/S3B findings, the extended J3/S6A tandem phase allows us to model the expected reduction in uncertainty over longer operational time frames. Statistically, the uncertainty of a temporal mean decreases proportionally to $1/\sqrt{n}$, where n is the number of observation cycles. Because both the S3A/S3B and J3/S6A tandem phases share an identical spatial and temporal configuration with a 30-second time delay between satellites, their uncertainty estimates show excellent consistency and follow the same statistical decay behaviour. However, the S3A/S3B tandem phase was relatively short. Therefore, we used the significantly longer J3/S6A tandem phase dataset to achieve a more robust empirical fit for the theoretical $1/\sqrt{n}$ decay model (Fig. 6, left panel). Relying on this validated baseline, we extrapolated the shorter S3A/S3B 4-hour tandem phase uncertainty curve into the future to establish operational requirements. The right panel of Fig. 6 illustrates the required number of days to reach specific target uncertainties. The horizontal thresholds act as visual guides for 1, 2, and 3-years mission durations. Using this extrapolation, we estimate that a 4-hour tandem phase would require approximately two years to reach the 2 mm precision achieved by a classical tandem phase in three months. However, intersecting the 4-hour tandem curve at the 1-year threshold yields an uncertainty of approximately 3.5 mm.

5.2 Comparison with dual-crossover approach

To assess the sensitivity and robustness of the along-track comparison methodology, we conducted a parallel analysis using a second method based on crossovers dual-crossovers between the two altimetric missions (see Fig. ??4).

The crossover-based dual-crossover-based method aggregates SLA difference values at these points for time lags below 10 days. This upper limit was chosen to ensure sufficient spatial coverage and data volume for statistically meaningful results. The differences are spatially averaged into $3° \times 3°$ grid cells, resulting in gridded MSL difference fieldsSLA difference fields, analogous to those derived from along-track comparisons. The regional SLA offset is then estimated by averaging the time series of each cell across multiple cycles. The associated uncertainty is calculated using the temporal method (described in Section 3.2.2), ensuring a homogeneous calculation with the other configurations presented in Fig. 4.

A key advantage of the crossover-based dual-crossover-based approach lies in its relative independence from the specific orbital configuration or tandem scenario. The method provides consistent results across different mission pairs, such as J3/S6A and S3A/S3B. This robustness to orbital configuration enhances the general applicability of the crossover dual-crossover technique and reinforces its relevance as a complementary method for altimetric continuity assessments. Over a one-year timescale, both configurations yield an uncertainty of approximately 6 mm, closely matching the results obtained outside the tandem phase for S3A/S3B.

5.3 Comparison of two uncertainty estimation methods

To further assess the consistency of uncertainty estimates, we apply both statistical methods described in Section 3.2 to a longer tandem phase available with the J3/S6A mission dataset. ~~The two methods for estimating regional offset uncertainty~~ A comparative summary of the uncertainty evolution derived from both methods is presented in Fig. 6. The primary conclusion drawn from this Figure is that both approaches yield highly consistent results, producing nearly identical uncertainty curves as the number of observation cycles increases. This strong agreement cross-validates the two techniques and improves confidence in the overall robustness of our continuity assessment framework. While both methods are valid, they each offer distinct advantages ~~and are suited for different purposes,~~ depending on the available data and the specific objectives of the analysis.

The first method, based on the spatial standard deviation of the regional offset field, is particularly well-suited when only a limited number of cycles are available. It allows for a rapid estimation of regional offset uncertainty and serves as an independent validation approach. Its simplicity and minimal data requirements make it especially useful for short-duration tandem phases or initial assessments. It is however sensitive to uncorrected systematic errors that could lead to an overestimation of the uncertainty.

The second method estimates uncertainty at the local scale by analysing the temporal variability of SLA differences within each grid cell. This approach aligns with global uncertainty assessment analyses, ensuring consistency between regional and global uncertainty assessments. One of its major advantages is the ability to produce spatially resolved uncertainty maps, facilitating the construction of detailed regional uncertainty budgets and enabling identification of geographically heterogeneous behaviours. Additionally, this method is less sensitive to systematic error corrections performed beforehand. By explicitly accounting for potential autocorrelation through the calculation of an effective sample size, this approach provides a more rigorous statistical interpretation. However, its reliability is constrained by the number of available cycles, particularly in short tandem phases.

Together, these two complementary uncertainty estimation approaches provide consistent results and improve confidence in the robustness of the continuity assessment framework. ~~A comparative summary of both methods is presented in Fig. ??.~~ However, because the temporal approach is mathematically consistent with the global mean uncertainty assessment, accounts for temporal correlation, and provides geographically resolved insights, we recommend the temporal approach, provided the tandem phase is long enough to supply a sufficient number of observation cycles.

6 Conclusions

This study addresses the critical issue of ensuring continuity in SLA measurements between successive S3 and S3NG-T altimetry missions. Traditional tandem ~~phase~~phases, where missions fly in close formation, are crucial for mission continuity. However, orbital constraints prevent a classic tandem phase between S3 and S3NG-T, necessitating a new approach with a 4-hour time delay between observations. The introduction of this 4-hour delay brings an additional source of uncertainty in offset estimation. Quantifying this uncertainty is essential to evaluate the feasibility and effectiveness of such a configuration for maintaining data continuity. In this study, we developed a technique to simulate the 4-hour delay using ~~crossovers~~

dual-crossovers with SWOT KaRIn data and assessed its impact by comparing multiple configurations, including scenarios with and without tandem phase, as well as different spatial and temporal sampling schemes. By analysing nearly one year of observations and implementing tailored statistical metrics, we quantified the continuity of SLA measurements between two missions and estimated the associated uncertainties. Beyond the methodological aspects, these findings have significant implications for ocean science and climate applications requiring long-term and stable satellite sea level data records. Our results demonstrate that sea level data continuity between S3 and S3NG-T is maintained despite a 4-hour delay instead of a classical near-simultaneous calibration phase. Although this 4-hour delay introduces short-term time-correlated effects due to ocean variability, we show that such effects can be effectively quantified and mitigated through an extended calibration period.

Specifically, while classic tandem configurations can achieve a 2 mm detectability threshold within three months, a 4-hour tandem phase would require approximately two years of continuous observations to reach a similar level of calibration precision~~(Fig. ??).~~ . However, the demonstrated ability to detect systematic differences of ±3.5 mm within one year highlights the feasibility of this approach. Consequently, the methodology developed ensures for users that future S3NG-T datasets will remain seamless and consistent with the existing S3 legacy, given the possibility of extending the tandem phase to one year.

Although this study focuses on SLA, the methodology is equally applicable to other key altimetric parameters such as significant wave height (SWH) and backscatter coefficient (σ_0). Since the primary objective of S3NG-T is to ensure the continuity of S3 measurements across all topographic products -ocean, inland water (rivers and lakes), sea ice, ice sheets, and atmospheric parameters- the approach developed here holds broad relevance. In addition, the study design supports regional analyses, allowing targeted assessments in specific ocean basins or geographic areas of interest.

A key limitation of the method developed in this study is that ~~SSHA~~ SLA differences at a 4-hour time lag reflect the combined effects of oceanic variability and altimetric measurement errors. These errors arise from multiple sources, including inaccuracies in environmental corrections such as ocean tides, atmospheric influences, and internal tide signals. Nonetheless, anticipated improvements in altimetric data processing and environmental ~~modeling~~ modelling over the next decade -such as enhanced tide models leveraging SWOT's high-resolution observations (Zhao, 2024)- are expected to significantly reduce these sources of uncertainty. As a result, future comparisons between S3NG-T and S3 will benefit from these advancements, enabling more precise assessments of mission continuity. An important perspective of this study is then the potential to isolate and quantify the respective contributions of oceanic variability and measurement errors to the overall uncertainty in SLA differences during a 4-hour tandem phase. Achieving such a separation would enable a more robust estimation of offset uncertainties and offer valuable insights into the nature and sources of altimetric errors.

Author contributions. N.L and M.A conceived the presented approach. N.L., M.A. and T.V. developed the theory and performed the computations. All authors discussed the results and contributed to the final manuscript.

Competing interests. None declared

Acknowledgements. This study was initiated as part of the S3NGT-MPUA project, supported by ESA. It also benefited from initial funding by CNES to develop the study's core concept. Additionally, the ASELSU project, also supported by ESA, contributed to improving the formalism used in this article to provide uncertainty estimates. All computational resources, including the use of specific libraries and data access, were facilitated by access to the CNES HPC cluster.

References

Ablain, M., Lalau, N., Meyssignac, B., Fraudeau, R., Barnoud, A., Dibarboure, G., Egido, A., and Donlon, C.: Benefits of a second tandem flight phase between two successive satellite altimetry missions for assessing instrumental stability, Ocean Science, 21, 343–358, https://doi.org/10.5194/os-21-343-2025, 2025.

Archer, M., Wang, J., Klein, P., Dibarboure, G., and Fu, L.-L.: Wide-swath satellite altimetry unveils global submesoscale ocean dynamics, Nature, 640, 691–696, https://doi.org/10.1038/s41586-025-08722-8, 2025.

AVISO/DUACS: SWOT Level-3 KaRIn Low Rate SSH Expert, https://doi.org/10.24400/527896/A01-2023.018, 2024.

Buijsman, M. C., Waterhouse, A. F., Zaron, E. D., Yadidya, B., Xu, C., Whitley, V., Wenegrat, J. O., Wang, J., Wallcraft, A. J., Varma, D., Tchonang, B. C., Siyanbola, O., Shriver, J. F., Sheremet, V. A., Send, U., Raja, K. J., Polzin, K., Ngodock, H. E., Moulin, A. J., Meiners, G., Lucas, A. J., Lankhorst, M., Kuehl, J. J., Kelly, S. M., Kachelein, L., Huang, Y., Griffin, C., Girton, J. B., Farrar, J. T., Delpech, A., Chen, Z., Chassignet, E. P., Carrier, M. J., Bracco, A., Arbic, B. K., Andres, M., and Abdulfatai, M. A.: A Multiagency Experiment on Internal Wave Energy, Mixing, and Interactions and Their Representation in Global Ocean Models and Operational Forecasts, Bulletin of the American Meteorological Society, 107, E158–E182, https://doi.org/10.1175/BAMS-D-24-0174.1, 2026.

Clerc, S., Donlon, C., Borde, F., Lamquin, N., Hunt, S. E., Smith, D., McMillan, M., Mittaz, J., Woolliams, E., Hammond, M., Banks, C., Moreau, T., Picard, B., Raynal, M., Rieu, P., and Guérou, A.: Benefits and Lessons Learned from the Sentinel-3 Tandem Phase, Remote Sensing, 12, 2668, https://doi.org/10.3390/rs12172668, 2020.

Cronin, M., Weller, R., Lampitt, R., and Send, U.: Ocean Reference Stations, in: Earth Observation, edited by Rustamov, R., InTech, ISBN 978-953-307-973-8, https://doi.org/10.5772/27423, 2012.

Dibarboure, G., Pujol, M.-I., Briol, F., Traon, P. Y. L., Larnicol, G., Picot, N., Mertz, F., and Ablain, M.: Jason-2 in DUACS: Updated System Description, First Tandem Results and Impact on Processing and Products, Marine Geodesy, 34, 214–241, https://doi.org/10.1080/01490419.2011.584826, 2011.

Dinardo, S., Maraldi, C., Daguze, J.-A., Amraoui, S., Boy, F., Moreau, T., and Picot, N.: Sentinel-6 MF Poseidon-4 Radar Altimeter In-Flight Calibration and Performances Monitoring, https://doi.org/10.24400/527896/A03-2022.3377, 2022.

Dorandeu, J., Ablain, M., Faugère, Y., Mertz, F., Soussi, B., and Vincent, P.: Jason-1 global statistical evaluation and performance assessment: Calibration and cross-calibration results, Marine Geodesy, 27, 345–372, https://doi.org/10.1080/01490410490889094, 2004.

Dufau, C., Orsztynowicz, M., Dibarboure, G., Morrow, R., and Le Traon, P.: Mesoscale resolution capability of altimetry: Present and future, Journal of Geophysical Research: Oceans, 121, 4910–4927, https://doi.org/10.1002/2015JC010904, 2016.

European Space Agency: Copernicus Sentinel-3 Next Generation Topography Mission Requirements Document, Tech. rep., European Space Agency, https://doi.org/10.5281/ZENODO.17454428, version Number: 1.0, 2025.

Guérou, A., Meyssignac, B., Prandi, P., Ablain, M., Ribes, A., and Bignalet-Cazalet, F.: Current observed global mean sea level rise and acceleration estimated from satellite altimetry and the associated measurement uncertainty, Ocean Science, 19, 431–451, https://doi.org/10.5194/os-19-431-2023, 2023.

Henry, O., Ablain, M., Meyssignac, B., Cazenave, A., Masters, D., Nerem, S., and Garric, G.: Effect of the processing methodology on satellite altimetry-based global mean sea level rise over the Jason-1 operating period, Journal of Geodesy, 88, 351–361, https://doi.org/10.1007/s00190-013-0687-3, 2014.

Leuliette, E., Nerem, R. S., and Mitchum, G. T.: Calibration of TOPEX/Poseidon and Jason Altimeter Data to Construct a Continuous Record of Mean Sea Level Change, Marine Geodesy, 27, 79–94, https://doi.org/10.1080/01490410490465193, _eprint: https://doi.org/10.1080/01490410490465193, 2004.

Masters, D., Nerem, R. S., Choe, C., Leuliette, E., Beckley, B., White, N., and Ablain, M.: Comparison of Global Mean Sea Level Time Series from TOPEX/Poseidon, Jason-1, and Jason-2, Marine Geodesy, 35, 20–41, https://doi.org/10.1080/01490419.2012.717862, 2012.

Morrow, R., Fu, L.-L., Ardhuin, F., Benkiran, M., Chapron, B., Cosme, E., d'Ovidio, F., Farrar, J. T., Gille, S. T., Lapeyre, G., Le Traon, P.-Y., Pascual, A., Ponte, A., Qiu, B., Rascle, N., Ubelmann, C., Wang, J., and Zaron, E. D.: Global Observations of Fine-Scale Ocean Surface Topography With the Surface Water and Ocean Topography (SWOT) Mission, Frontiers in Marine Science, 6, 232, https://doi.org/10.3389/fmars.2019.00232, 2019.

Nilsson, J., Desai, S., Desjonqueres, J.-D., and Haines, B.: Global cross-calibration of the Jason-3 and Sentinel-6 Michael Freilich missions during their tandem period, https://doi.org/10.24400/527896/A03-2022.3354, 2022.

Prandi, P., Meyssignac, B., Ablain, M., Spada, G., Ribes, A., and Benveniste, J.: Local sea level trends, accelerations and uncertainties over 1993–2019, Scientific Data, 8, 1, https://doi.org/10.1038/s41597-020-00786-7, 2021.

Rieu, P., Moreau, T., Cadier, E., Raynal, M., Clerc, S., Donlon, C., Borde, F., Boy, F., and Maraldi, C.: Exploiting the Sentinel-3 tandem phase dataset and azimuth oversampling to better characterize the sensitivity of SAR altimeter sea surface height to long ocean waves, Advances in Space Research, 67, 253–265, https://doi.org/10.1016/j.asr.2020.09.037, 2021.

Sentinel-3 and Jason-CS-Sentinel-6 Product Handbook: Along-track Level-2+ (L2P) Sea Level Anomaly Sentinel-3 / Jason-CS-Sentinel-6 Product Handbook, https://www.aviso.altimetry.fr/fileadmin/documents/data/tools/hdbk_L2P_S3_S6.pdf, 2022.

Zawadzki, L. and Ablain, M.: Accuracy of the mean sea level continuous record with future altimetric missions: Jason-3 vs. Sentinel-3a, Ocean Sci., 12, 9–18, https://doi.org/10.5194/os-12-9-2016, 2016.

Zhao, Z.: Internal Tides From SWOT: A 75-Day Instantaneous Mode-1 M2 Internal Tide Model, Journal of Geophysical Research: Oceans, 129, e2024JC021 174, https://doi.org/10.1029/2024JC021174, 2024.

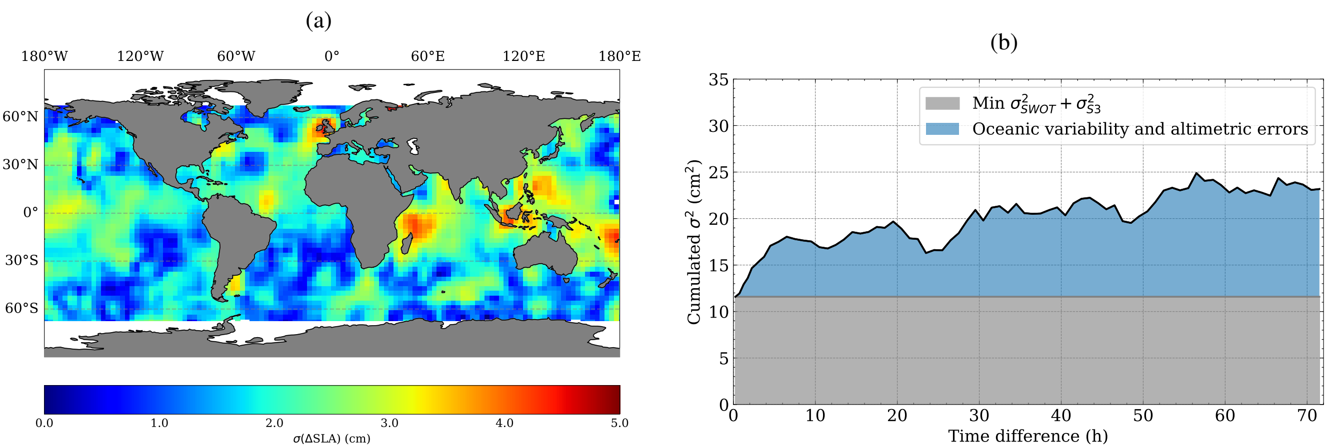

Figure 1. (a) Map of variability in 4-hours time interval, from SWOT KaRIn and S3A and S3B dual-crossovers and (b) Time series of the cumulated variance of ΔSLA ; decomposition between instrumental errors (grey) and oceanic variability (blue).

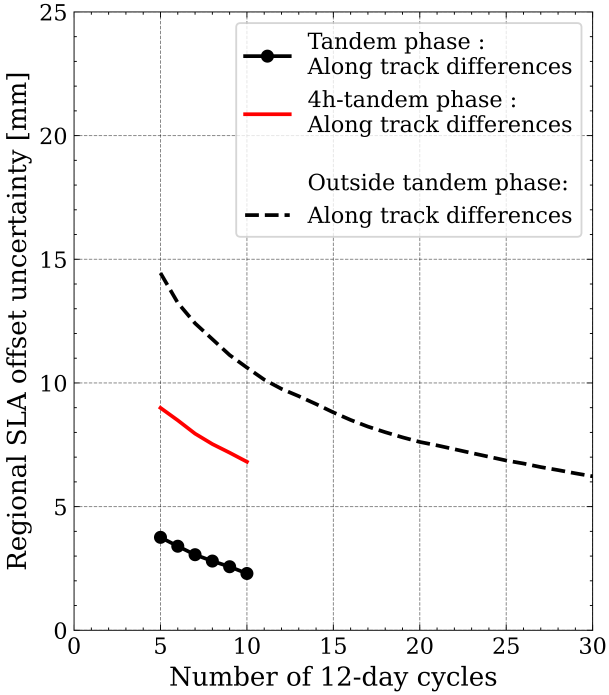

Figure 2. S3A and S3B regional SLA offset uncertainties on 3x3° grid for 12-day subcycles–. Uncertainties are computed using the temporal method for along-track comparison methods with three different configurations: classical tandem phase, 4h-tandem 4-hour tandem phase, and outside tandem phase.

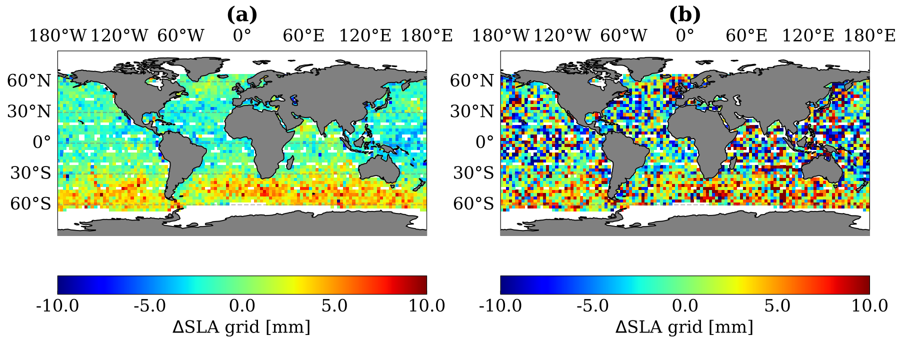

Figure 3. Differences between S3A and S3B for (a) Classical tandem phase for 3*3° boxes and (b) 4-hours tandem phase for 3*3° boxes

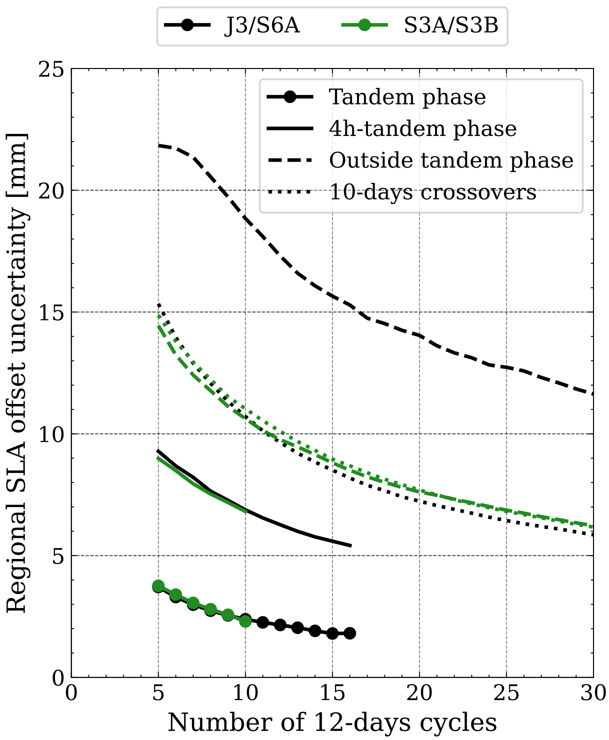

Figure 4. J3/S6A (black) and S3A/S3B (green) regional SLA offset uncertainties on 3x3° grid for 12-day subcycles, . Uncertainties are computed using the temporal method for four different comparison methodsconfigurations: tandem phase, 4h-tandem phase, outside tandem phase and 10-days crossoversdual-crossovers.

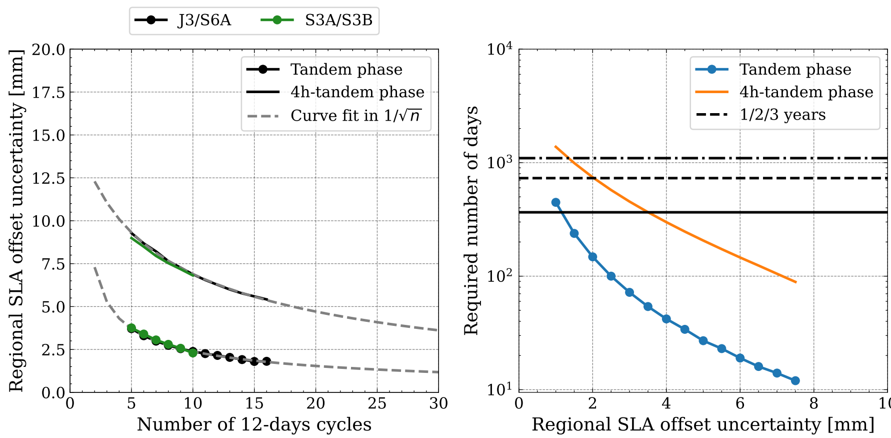

Use of the J3/S6A comparison during the tandem phase to fit the uncertainty evolution (left figure) and to estimate the number of days (right figure) required for the 4-hour tandem phase (orange) to reach the same precision as the classical tandem phase (blue). The horizontal black lines indicate, from bottom to top, the 1-, 2-, and 3-year thresholds.

Use of the J3/S6A comparison during the tandem phase to fit the uncertainty evolution (left figure) and to estimate the number of days (right figure) required for the 4-hour tandem phase (orange) to reach the same precision as the classical tandem phase (blue). The horizontal black lines indicate, from bottom to top, the 1-, 2-, and 3-year thresholds.

Figure 5. ~~Comparison of two uncertainty estimation methods for J3/S6A in a regional analysis using a 3°×3° grid resolution.~~
Use of the J3/S6A comparison during the tandem phase to fit the uncertainty evolution (left figure) and to estimate the number of days (right figure) required for the 4-hour tandem phase (orange) to reach the same precision as the classical tandem phase (blue). The horizontal black lines indicate, from bottom to top, the 1-, 2-, and 3-year thresholds.

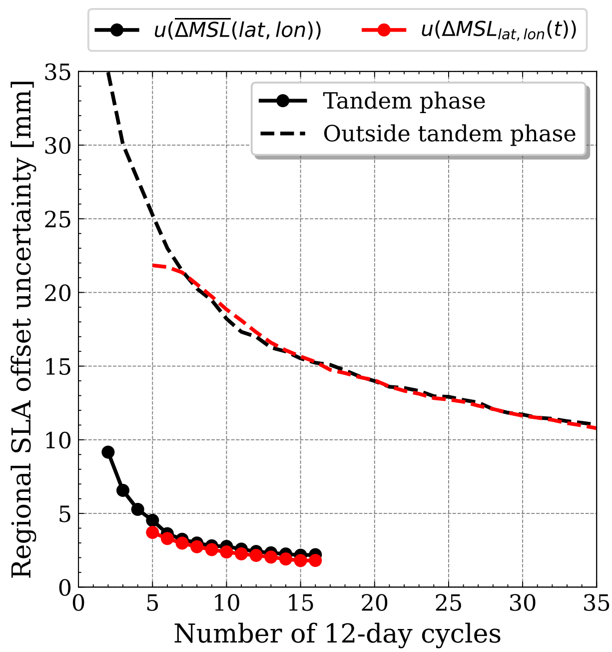

Figure 6. Differences between S3A and S3B Comparison of two uncertainty estimation methods for (J3/S6A in a) Classical tandem phase for 3*3regional analysis using a 3°boxes and (b) 4-hours tandem phase for 3*3×3° boxesgrid resolution.

Map of variability in 4-hours time interval

Table A1. Summary of the gridded datasets generated for each scenario.

Scenario	**SLA Grids** [$3^\circ \times 3^\circ$, **12 days**] **(Individual Missions)**	**ΔSLA Grids** [$3^\circ \times 3^\circ$, **12 days**] **(Mission Pairs)**
Classical Tandem phase	S3A, from SWOT KaRIn S3B, J3, S6A	S3A/S3B and J3/S6A
Outside tandem phase	S3A, S3B, J3, S6A	S3A/S3B and J3/S6A
4-hour tandem phase	S3A, S3Bcrossovers., J3, S6A	S3A/S3B and J3/S6A